Chapter 6

Bell-mouth with tapered collector for high temperature applications

The bulk movement of fluid in natural convection solar air heater (SAH) is generated due to density variation and hence suffers from lower mass flow rates. Mounting additional surfaces/fins in SAH duct enhances the thermal characteristics, however, it comes at the cost of hydraulic performance. This limits the device usage in buildings and other high flow rate applications. In the present chapter, two new designs of SAH were numerically analyzed are: (a) taper flow passage for better thermal performance; (b) tapered designs incorporated with bell-mouth inlet opening for improved hydraulic performance. Parametric design analysis was conducted for large range of taper ratio and bell-mouth ratio. The results show that the tapered design is about 70% thermally more effective and about 6% higher Nusselt number per unit pressure drop than conventional SAH. A significant enhancement in hydraulic performance of more than 300% was observed when bell-shaped inlet design was integrated with the tapered designs. An independent correlation for Nusselt number variation has been developed as a function of Rayleigh number and tapper ratio. Predictions from the developed correlation is in excellent following with the numerical data.

6.1 Introduction

Solar energy is a vast source of energy received in the form of solar radiation, if utilized efficiently, can save millions of tons of carbon dioxide released by burning of fossil fuels. This clean energy resource is environment-friendly and easily available in daylight hours. Solar radiation available in day time used to serve many applications all around the world, such as air heating [133], water heating [112], crop drying [121], and many other domestic and industrial applications. The solar air heater (SAH) is a device used for fluid (air) heating when it passes through a SAH flow channel. Two types of SAH are generally classified based on the mode of fluid circulation: (a) forced convection [40, 164] and (b) natural convection [151, 91]. In forced convection, SAH fluid is pumped by an external agency such as air blower, centrifugal pump etc. [140, 89], while in natural convection, the flow is naturally driven by buoyancy forces generated due to variation in the fluid density [9, 18]. In forced convection mode the electrical power consumption is substantially higher which increases the cost per unit mass of heated air [2, 83]. Further, installation is a major concern in the regions where electricity supply is intermittent. Due to these issues associated with forced convection SAH, the research community prefer to focus on thermo-hydraulically efficient designs of naturally driven devices that operates on natural convection mode for wide acceptability of the device in various applications. A natural convection SAH is a self-driven device works under the principle of fluid density gradient [139], and hence no external mechanical/electrical power requirement for its operation.

Many previous studies have reported improvement in thermal characteristics of natural convection SAH devices by mounting fins or extended surface inside the flow channel [53, 119]. These protruding surfaces from the absorber plate, though enhances the thermal performance, effects the hydraulic efficiency significantly. The obstruction offered to naturally driven flow in the SAH duct reduces the mass flow rate of heated air considerably. Decrease in the flow rate adversely affects the device suitability for high mass flow rate applications such as crop

drying [121, 131], space heating [84, 64, 96], etc. The enhanced thermo-hydraulic performance by changing the flat smooth flow passage into curved flow passage without ribs or extended surfaces has been reported earlier [141, 142, 138]. However, thermally and hydraulically efficient designs of smooth flat plate SAH without the integration of any extended surfaces is yet to be investigated in detail.

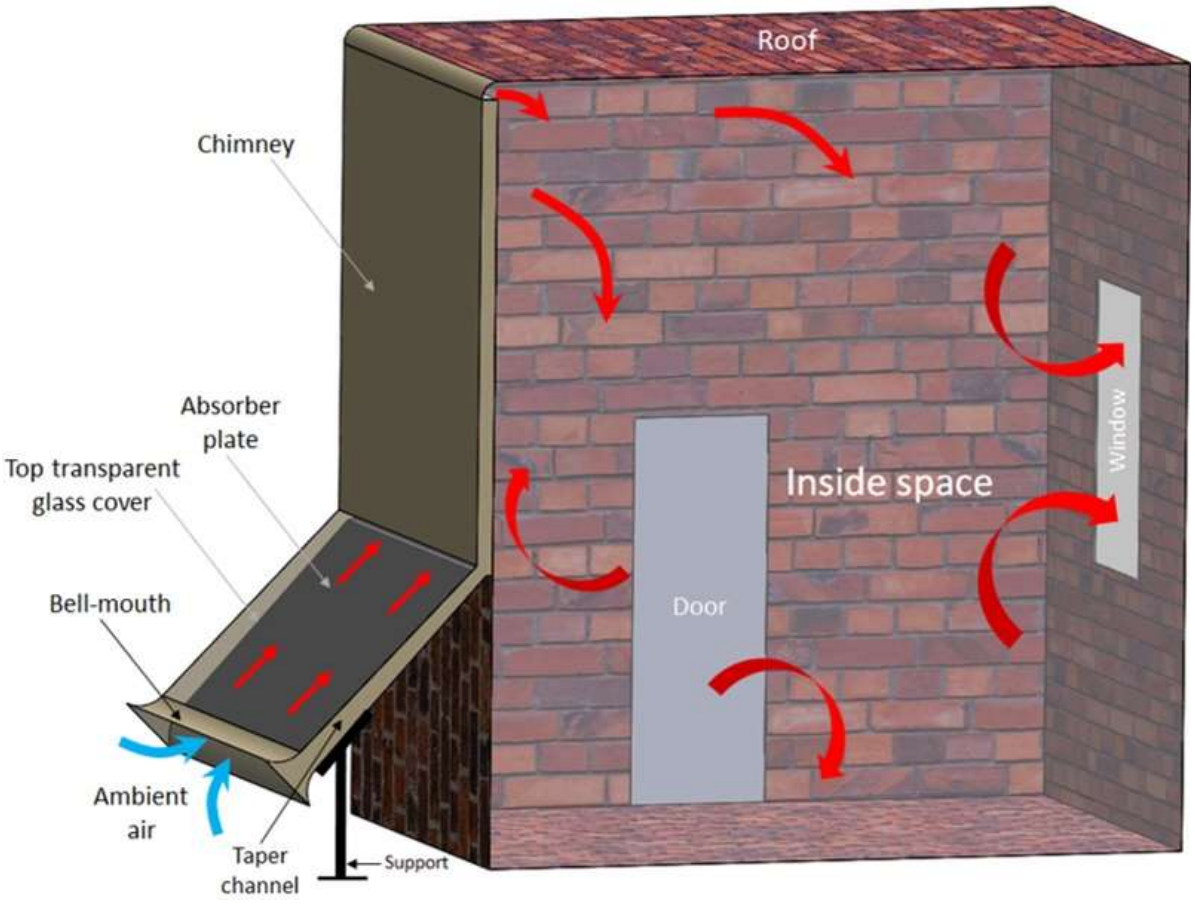

Figure 6.1: Tapered SAH with bell-mouth integrated with building for space heating and ventilation.

Since 50% of the electrical energy is used in the building and heating application [106], many investigators have proposed innovative techniques to reduce the heating and cooling loads in buildings [23]. Hussain et al. [8] investigated effect of different inlet designs of roof top solar chimney. However, their study was limited to changing the direction inlet plane. Many investigations have been done on coupling SAH for buildings ventilation [22, 81]. Some recent studies show that thermal storage mechanisms such phase change materials are also being use to harness solar energy for building applications [23].

In the present study, the thermal performance has been enhanced and later hydraulically efficient system designs were presented and analyzed. The tapered flow passage increases the thermal performance of the device at the expense of mass flow rate, and further, this decrease in the mass flow rate has been compensated by integrating bell-mouth designs at the inlet of SAH. Integrating bell-mouth at the inlet attenuate hydraulic entry losses [137]. The two novel designs of natural convection SAH have been reported here: (i) the parallel flow passage has been transformed to tapered flow passage for the applications where high temperature is the primary requirement, and (ii) bell-mouth design integrated at the inlet of tapered SAH for enhanced hydraulic performance to achieve higher mass flow rate for high flow rate applications. Both the above cases were individually studied and it was observed that the first design is about 70% better in terms of thermal performance, and second design with bell-mouth inlet boosted the mass flow rate by more than three folds i.e. about 313% when compared with conventional SAH design.

The proposed system design (see Fig. 6.1) would be much better for applications where high-temperature fluid with high mass flow rate is the primary requirement, such as building heating, natural ventilation, solar dryer, etc. Although water heating systems for building applications are widely used and accepted due to their ease of placement on the roof, integrating a SAH device for building air heating is yet to take off due

to their low mass flow rates and low efficiency. If suitably designed as shown in schematic Fig. 6.1, high flow SAH can occupy one of the walls for heating the air before it enters the building. The design is comparatively less complicated compared to the Trombe wall. To maintain proper natural ventilation, the low-temperature ambient air enters the SAH finally exit from the window after heating the inside living space (see Fig. 6.1). The proposed designs of natural convection SAH are thermo-hydraulically much better than the conventional systems and would assist researchers and industry in developing such a promising self-operated device.

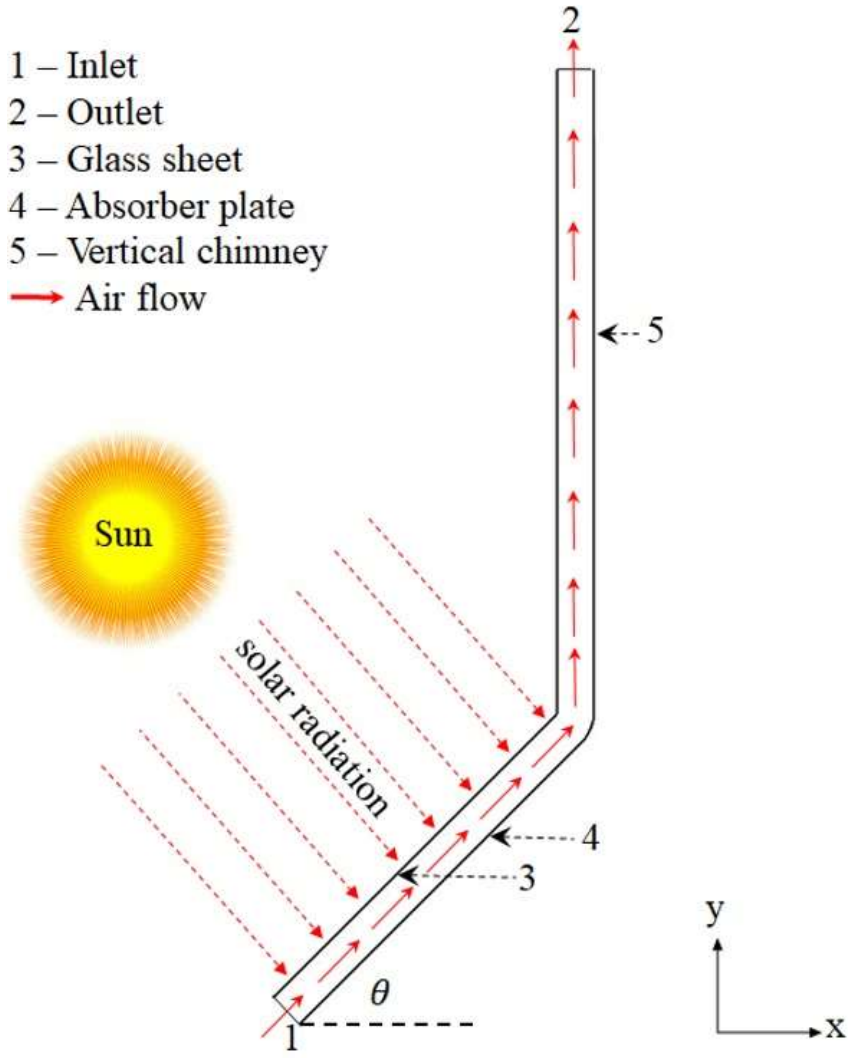

Figure 6.2: Conventional design of natural convection SAH having parallel flow passage at an inclination angle (θ) of 45° .

6.2 Description of the problem

In the present study design of conventional natural convection SAH (see Fig. 6.2) comprise of a parallel smooth flow channel integrated with a vertical chimney. The flow passage has a glass plate at the top and an absorber plate at the bottom. In the new design, the parallel flow passage is redesigned to a tapered flow passage (see Fig. 6.3). Dimension H_1 denotes the opening width of the flow channel and H_2 is the width at the SAH exit section. The tapered SAH performance has been evaluated for various values of taper ratios H_2/H_1 in the range $0.5 - 0.89$. Figure 6.4 shows the design of naturally driven SAH incorporated with bell-mouth inlet opening. Each case of tapered SAH in Fig. 6.3 are examined by integrating various designs of bell-mouth shape opening at the SAH inlet. The range of bell-mouth ratio considered was $h/R = 0.1 - 0.6$, where h stands for perpendicular distance from either side (top glass surface/insulated bottom) of the flow channel at the inlet section and R is the bell-mouth curvature radius. All design parameters are enlisted in Table 6.1. This analysis was performed in the northern part of India, which falls approximately 30°average latitude, and hence our model

was set at (30°+ 15° (winter) = 45°) inclination. Further, our model is based on the work of Gilani et al. [53], in which they reported 45°inclination. It has also been reported [119] that when a SAH is inclined at 45°, its thermal performance is highest for naturally driven systems. The detailed description of the thermo-hydraulic performance of the new SAH designs have been reported in the result and discussion section.

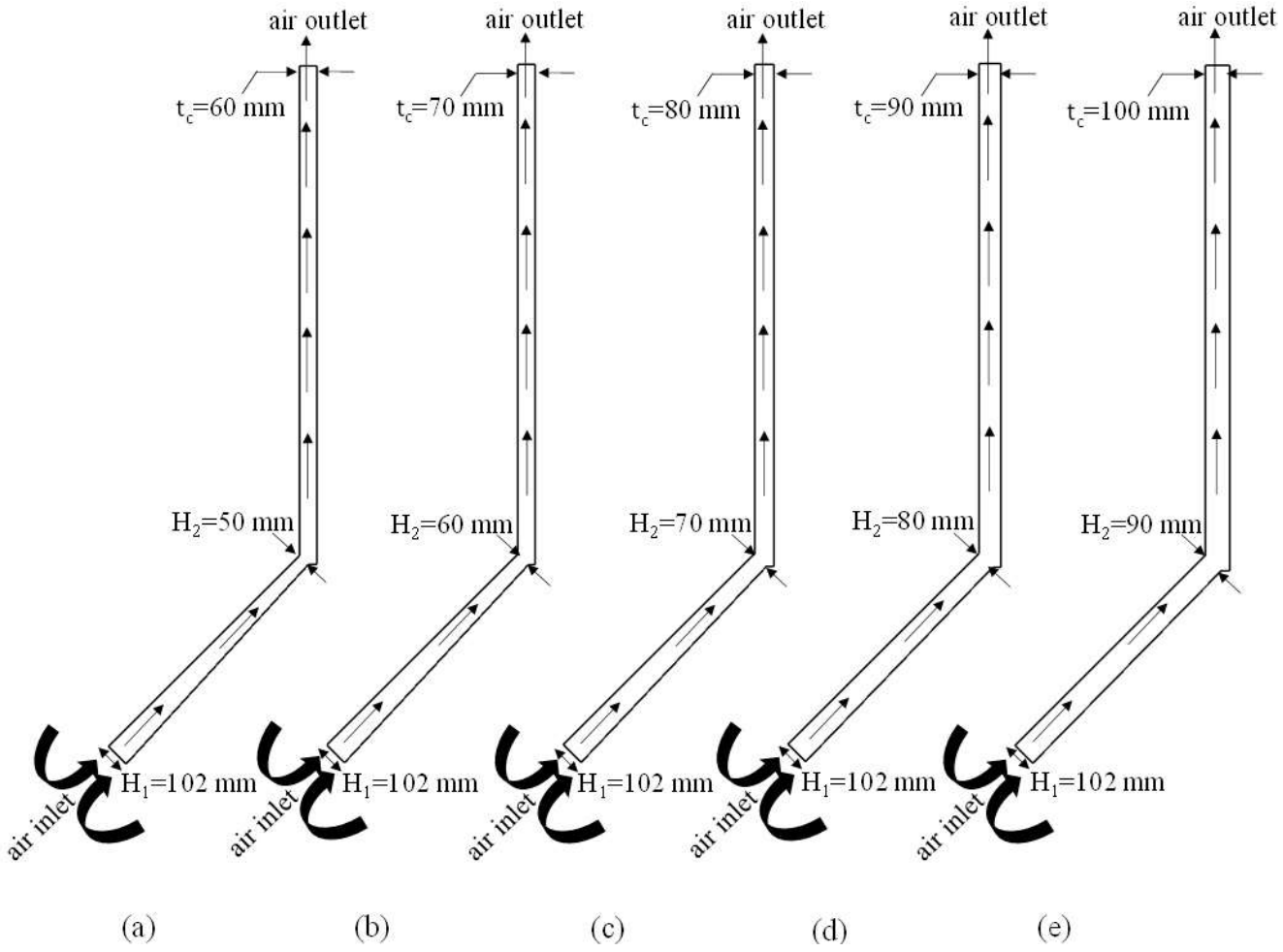

Figure 6.3: Natural convection tapered SAH inclined at $\theta = 45^\circ$, integrated with a vertical chimney. Note that while the dimension of inlet passage is kept constant, outlet width of SAH and chimney was varied. The dimensions are: (a) $H_1 = 102mm$, $H_2 = 50mm$ & $t_c = 60mm$ (b) $H_1 = 102mm$, $H_2 = 60mm$ & $t_c = 70mm$, (c) $H_1 = 102mm$, $H_2 = 70mm$ & $t_c = 80mm$, (d) $H_1 = 102mm$, $H_2 = 80mm$ & $t_c = 90mm$, (e) $H_1 = 102mm$, $H_2 = 90mm$ & $t_c = 100mm$.

The SAH comprises of tapered flow passage integrated with a vertical chimney has been investigated for two different designs of inlet section: (i) uniform rectangular cross-sectional shape inlet and (ii) inlet integrated with bell-mouth shape. The SAH is 1100 mm in length and chimney height is 2000 mm, the opening width at the inlet section i.e. H_1 is 102 mm. Higher chimney width results in reverse flow at chimney exit while a narrower width results in excessive frictional losses due to thermal boundary layer interaction. Hence, the opening width of the chimney outlet i.e. H_2 is made slightly 10 mm wider than the SAH exit opening to ensures smooth fluid flow movement without obstruction. The chimney is installed at the SAH exit section to enhance the updraft generated to drive the flow through the SAH duct. The design parameters are taper ratio of the flow passage i.e. H_2/H_1 and bell-mouth ratio, h/R. The geometrical parameters range are provided below in Table 6.1. The absorber plate was maintained at constant heat flux, and air enters the inlet section gets heated up and rises upward due to buoyancy forces generated due to density variation of the fluid. The thermal and hydraulic characteristics of the device varies with the change in design parameters which have been reported in the present study.

Table 6.1: Operating and geometrical parameters.

S. No.	Parameters	Range/value
1	Taper flow passage (see Fig. 6.3), all dimensions in 'mm'	H_1=102 to H_2=50; H_1=102 to H_2=60; H_1=102 toH_2=70; H_1=102 to H_2=80; H_1=102 toH_2=90; H_1=102 to H_2=102
2	Absorber plate heat flux (q) in W/m^2	500, 600, 700, 800, 900, 1000, 1100
3	Air velocity at the air inlet section	stagnation state (i.e. standstill condition)
4	SAH inclination angle with reference to horizontal plane (θ)	45° (fixed)
5	Bell-mouth ratio, h/R	0.1-0.6

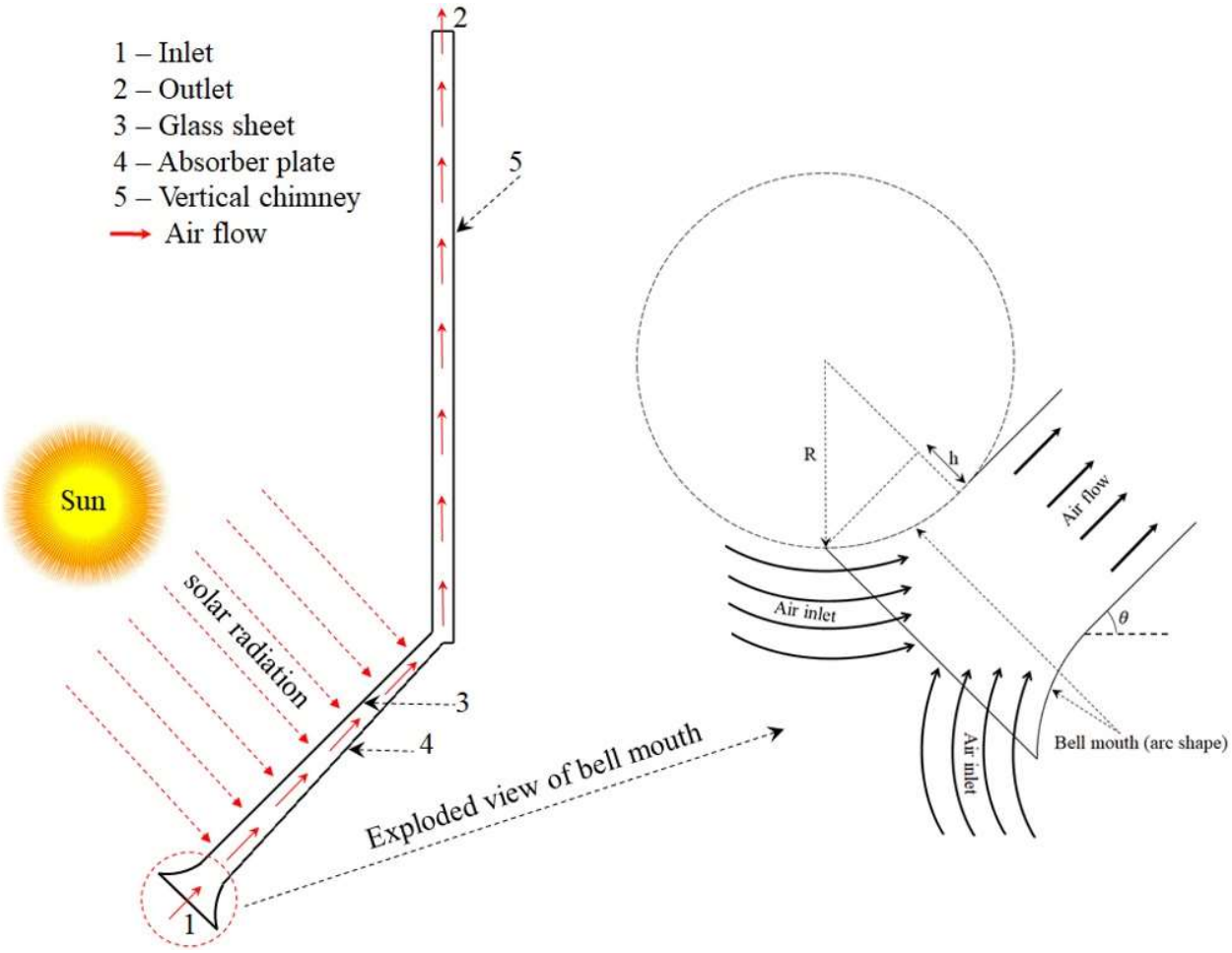

Figure 6.4: Natural convective tapered SAH united with bell-mouth shape inlet. The enlarged view of bell-mouth inlet opening is shown on the right. Each design of tapered SAH shown in Fig. 6.3 are individually analysed to understand the influence of bell shape opening on the performance of the device.

6.2.1 Mesh generation and grid independency test

Mesh generation is an important procedural step to discretize the domain into finite number of elements in such a way to obtain results with higher accuracy. The selection of grid size and shape has to be such that it achieves set convergence level in optimum time duration and less computational resources. In the present study two-dimensional computational flow domain was discretized using tria shape element. Unstructured mesh was generated for better capturing the flow vortices in the flow field. Fine mesh near the walls was created to accurately predict the heat transfer coefficient and shear stresses (see Fig. 6.5). The dimensionless wall distance (y^+) was maintained below unity. Numerical analysis and modeling have been done using HyperWorks software.

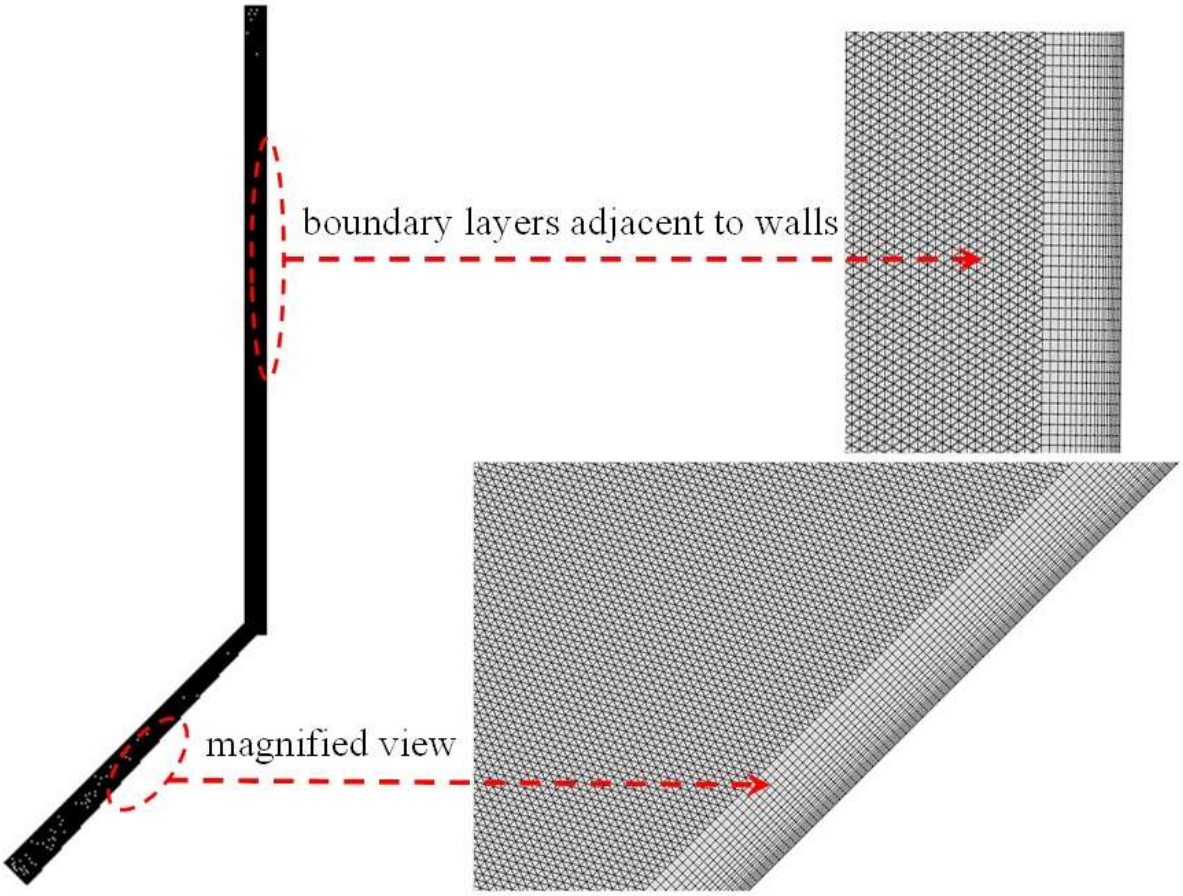

Figure 6.5: Meshed geometry of the numerical domain of tapered natural convection solar air heater. Magnified view shows boundary layer mesh near the heated absorber plate and chimney.

The test for grid independency of the identical numerical domain has already been conducted in the literature [141] by the same authors. For detailed information about the mesh generation and grid independent test readers can see Appendix A of the previous published work [141]. To keep the manuscript brief, details of the grid-independent study are not presented here.

6.2.2 Boundary conditions

The accurate numerical results depend on the boundary conditions imposed over the computational domain. At the inlet, air is at standstill condition (total pressure, P_{total}= 0) to mimic the environmental condition where magnitude of wind velocity is zero. The absorber plate was maintained at constant heat flux (q). To account the convection and radiation losses from the top glass surface, the top glass surface has subjected to heat transfer coefficient value $h = 5.7 + 3.8V_\infty$ W/m^2-K [150, 154], where V_∞ is ambient wind speed, which is assumed zero for stagnation condition. The static pressure at the outlet section was set to zero. Rest surfaces of the flow domain were considered as adiabatic wall. Flow prediction using Boussinesq approximation changes when the temperature gradient of walls exceeds 30°C [85, 168]. Considering the above fact, the fluid density variation has been modeled as the function of temperature $P = \rho.R.T$ i.e. ideal gas law behavior to take care the effect

of temperature variation on the fluid density.

The thermophysical properties of ambient air at 298 K at the SAH inlet are mentioned in Table 6.2.

Table 6.2: At the SAH inlet ambient air properties at 298 K are:

Properties name	Value
Dynamic viscosity (μ)	1.855 x 10-5 Ns/m^2
Thermal conductivity (k)	0.026 W/m K
Prandtl number (Pr)	0.71
Specific heat (C_P)	1003.62 J/kg K
Density (ρ)	1.184 kg/m^3

6.2.3 Non-dimensionless parameters and governing equations

The thermo-hydraulic characteristics were evaluated by analyzing the flow field in the form of temperature of air at the outlet section (T_o), Nusselt number (Nu) and mass flow rate (m). The Nu denotes the rate at which heat exchange occur from the absorber plate to flowing fluid. The mathematical formulation of Nusselt number [141] is given as:

$$Nu = \frac{h\ D_H}{k_a} \tag{6.1}$$

where D_H denote hydraulic diameter at the SAH inlet, h is the convection heat transfer coefficient (W/m^{2}K) and $k_a$is the thermal conductivity of air (W/m.K).

The thermal performance has been evaluated using thermal enhancement ratio, TER. It is defined as the ratio of outlet air temperature of the tapered SAH to the conventional SAH as-defined in Eq. 6.2,

$$TER = \frac{T_{o,\ \text{tapered}}}{T_{o,\ \text{flat}}} \tag{6.2}$$

The thermal efficiency of a device can be expressed in terms of thermal effectiveness (ε) which indicate thermal performance of the device can be expressed as the ratio of the actual rise in temperature to the maximum rise possible [141], i.e.

$$\varepsilon = \frac{(T_o - T_i)}{(T_s - T_i)} \tag{6.3}$$

Higher value of ε indicates a thermally efficient SAH design.

In the natural convection SAH, the flow movement occurs due to buoyancy forces generated because of change in fluid density. The dimensionless Rayleigh number, Ra values have been calculated based on the thermal and flow characteristics of the device working under natural convection mode. The non-dimensionless Rayleigh number (Ra) has been determined using Eq. 6.4 [53, 91, 119, 141].

$$Ra = \frac{\rho^2 \beta C_P g \Delta T L^3}{\mu k_a} \tag{6.4}$$

where ρ is the fluid (i.e. air) density, β denote volumetric expansion coefficient (K^{-1}), μ denote dynamic viscosity of fluid (kg/m.s), $\Delta T = T_s - T_a$ (K) where T_s = mean temperature of the absorber plate (K) and T_a= surrounding temperature (K), g is the acceleration due to gravity (m.s^{-2}), C_P denote air specific heat at constant pressure (J/kg.K) and k_a denote thermal conductivity of air (W/m.K). The non-dimensional number Ra plays an important role as it is directly proportional to the average temperature of the absorber plate. Higher the absorber surface temperature larger would be the magnitude of buoyancy forces which accelerates the flow at higher velocity. The values of Ra are used to predict the laminar and turbulent flow behavior in case of the buoyancy-driven flow. The values of Ra in the present analysis are of the order 10^{10} which denotes the flow in turbulent region, and hence in study the realizable K-Epsilon turbulent model [110, 124, 116] was selected for further simulations. The realizable K-Epsilon model resolves the flow field accurately at all dimensionless wall distance (y^+) with full buoyancy effect. The finite volume method (FVM) has been used to discretize the

governing equation. The second-order upwind scheme was used for velocities at control volumes interfaces. The numerical data obtained when parametric variation is insensitive to successive time steps.

The governing equations for the two-dimensional numerical domain are mentioned below:

Continuity equation

$$\frac{\partial \rho}{\partial t} + \frac{\partial (\rho u)}{\partial x} + \frac{\partial (\rho v)}{\partial y} = 0 \tag{6.5}$$

Momentum equations

$$\frac{\partial (\rho u)}{\partial t} + \frac{\partial (\rho u u)}{\partial x} + \frac{\partial (\rho u v)}{\partial y} = -\frac{\partial p}{\partial x} + \frac{\partial}{\partial x}\left[(\mu + \mu_t)\frac{\partial u}{\partial x}\right] + \frac{\partial}{\partial y}\left[(\mu + \mu_t)\frac{\partial u}{\partial y}\right] - \frac{2}{3}\rho\frac{\partial k}{\partial x} \tag{6.6}$$

$$\frac{\partial (\rho v)}{\partial t} + \frac{\partial (\rho u v)}{\partial x} + \frac{\partial (\rho v v)}{\partial y} = -\frac{\partial p}{\partial y} + \frac{\partial}{\partial x}\left[(\mu + \mu_t)\frac{\partial v}{\partial x}\right] + \frac{\partial}{\partial y}\left[(\mu + \mu_t)\frac{\partial v}{\partial y}\right] - \frac{2}{3}\rho\frac{\partial k}{\partial y} - (\rho - \rho_0)\, g \tag{6.7}$$

Energy equation

$$\frac{\partial (\rho T)}{\partial t} + \frac{\partial (\rho u T)}{\partial x} + \frac{\partial (\rho v T)}{\partial y} = \frac{\partial}{\partial x}\left[\left(\frac{K}{C_P} + \frac{\mu_t}{Pr_t}\right)\frac{\partial T}{\partial x}\right] + \frac{\partial}{\partial y}\left[\left(\frac{K}{C_P} + \frac{\mu_t}{Pr_t}\right)\frac{\partial T}{\partial y}\right] \tag{6.8}$$

where k is the turbulent kinetic energy, μ_t is the turbulent viscosity and Pr_t is the turbulent Prandtl number which is the ratio of eddy diffusivity for momentum $\left(\varepsilon_M = \frac{\overline{-u'v'}}{\frac{\partial u}{\partial y}}\right)$ and heat transfer $\left(\varepsilon_H = \frac{\overline{-v'T'}}{\frac{\partial T}{\partial y}}\right)$. The equations for turbulent kinetic energy and dissipation are:

$$\frac{\partial (\rho k)}{\partial t} + \nabla \cdot \left(\rho k \overline{V}\right) = \nabla \cdot \left[\left(\mu + \frac{\mu_t}{\sigma_k}\right)\nabla k\right] + G_k + G_b - \rho\varepsilon - \gamma_M + S_k \tag{6.9}$$

$$\frac{\partial (\rho \varepsilon)}{\partial t} + \nabla \cdot \left(\rho \varepsilon \overline{V}\right) = \nabla \cdot \left[\left(\mu + \frac{\mu_t}{\sigma_\varepsilon}\right)\nabla \varepsilon\right] + C_{\varepsilon 1}\frac{\varepsilon}{k}\left(G_k + C_{\varepsilon 3} G_b\right) - C_{\varepsilon 2}\rho\frac{\varepsilon^2}{k} - R_\varepsilon + S_\varepsilon \tag{6.10}$$

G_k and G_b represent turbulent and buoyancy generation, respectively.

where $\sigma_T = 1.0$, $\sigma_k = 1.0$, and $\sigma_\varepsilon = 1.2$, whereas constants $C_{\varepsilon 1} = 1.44$, $C_{\varepsilon 2} = 1.9$ and $C_\mu = 0.09$, where $Pr_t = 0.9$.

The velocity and pressure fields for the discretized flow domain were solved using SIMPLE (semi-implicit method for pressure linked equations) algorithm. The order of convergence was fixed to 10^{-3} for energy equation and 10^{-5} for velocity component and momentum equations.

6.3 Results and discussions

6.3.1 Effect of tapered flow channel on thermal performance

It was observed that in conventional SAH design, the thermal boundary layer is thin and confined near to the hot absorber surface. The major portion of the cold fluid just passes out the channel without interacting with the heated absorber plate. The flow channel was redesigned to a taper design as shown in Fig. 6.3 to bring colder fluid at the top of the channel near to the absorber plate to take advantage of diffusion and convection phenomena. The motivation to investigate such designs was to make high energy fluids in the boundary layer to interact with adjoining cold fluid layers without using extended surfaces. However, close proximity of plates increases boundary layer interaction resulting in higher frictional losses. These losses are compensated by integrating a bell-mouth design at the inlet (discussed later).

The cross-section of the flow passage is gradually converging along the length, as air accelerates in the tapered flow channel. The flat tapered flow passage shows a significant increase in the thermal characteristics compared to conventional parallel flat natural convection SAH in terms of T_o and Nu. The Figs. 6.6 and 6.7 shows the variation of thermal enhancement ratio (*TER), i.e.* $T_{o,\,\text{tapered}}$ / $T_{o,\,\text{flat}}$ and Nusselt number (Nu) for the range of $q = 500 - 1100$ W/m^2, respectively of tapered SAH. The taper passage is gradually converging type, which provides avenues for colder air at the upper part to come under frequent interaction of hot absorber

surface, and consequently, its effect can be seen in the form of increased heat transfer rate (see Figs. 6.6 and 6.7). In Fig. 6.6, the values of TER vary parabolically with heat flux for tapered SAH, having minimum values for smallest taper ratio i.e. 0.5 and consistently increases with increase in the taper ratio till 0.69. However, further increase in the taper ratio from 0.69 results in decrease of TER values. The maximum percentage increase of 14% is observed for the taper ratio 0.69. These results show effectiveness of the flat tapered flow passage over conventional flat plate parallel flow passage natural convective SAH. The slight modification of flat parallel flow passage into tapered flow passage shows considerable augmentation in the thermal performance.

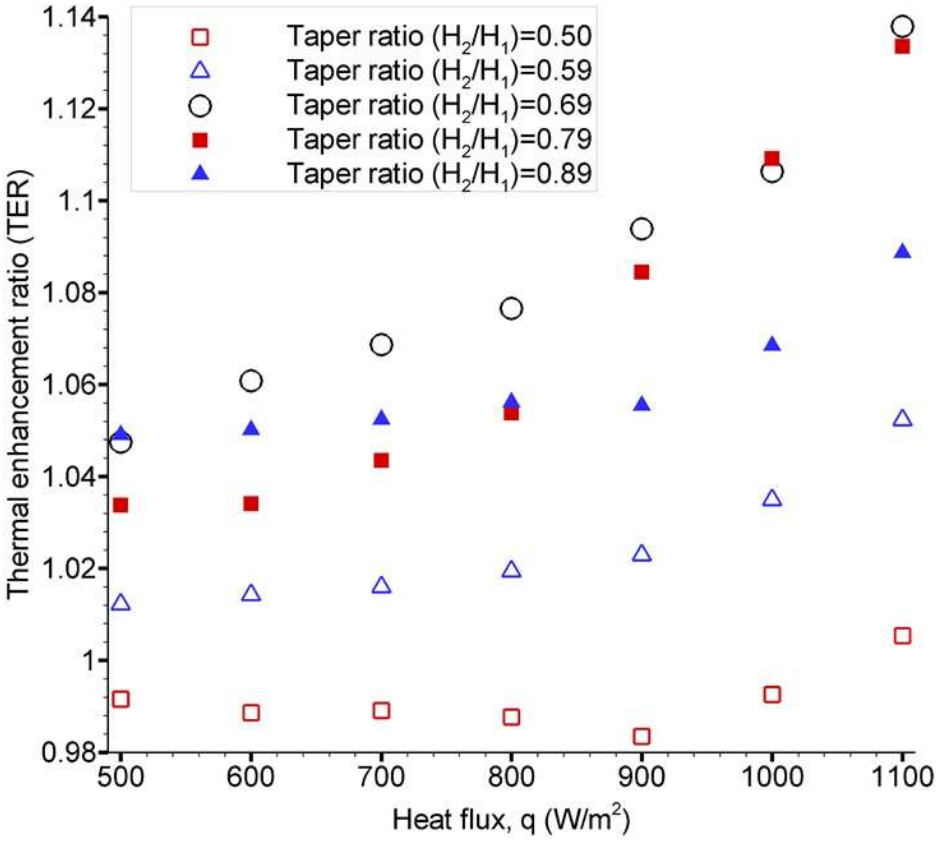

Figure 6.6: Variation of thermal enhancement ratio (TER) with heat flux (q) for tapered flow passage natural convection SAH.

Figure 6.7 demonstrates the variation of Nu vs. Ra for tapered SAH corresponding to the range of taper ratio $\frac{H_2}{H_1} = 0.5 - 1$. The higher values of Nusselt number were observed for tapered SAH with decreasing value of taper ratio due to greater flow velocity in the duct. The increased interaction of the cold fluid at the top with the absorber plate results in higher temperature gradient and hence the heat transfer rate. It is interesting to note that the Nu for taper ratio 0.89 is lower than taper ratio 1 (see Fig. 6.7) due to low-temperature gradient between fluid layers, but result changes significantly when a bell-shaped inlet is integrated with the SAH (Fig. 6.13). Without bell-mouth, taper ratio 0.89 shows less than 2% lower Nu than taper ratio 1 across the range of Rayleigh numbers. The new tapered SAH designs show significant enhancement in the thermal performance when compared to conventional SAH design.

Figure 6.8 shows mass flow rate variation with Rayleigh number of tapered flow passage SAH having rectangular inlet cross-section. Mass flow rate has parabolic variation with taper ratio, initially decreases with increase in H_2 value and attains minimum, and increases afterwards. The decrease in flow velocity provides sufficient time for the flowing fluid to interact with the hot absorber plate which enhances the temperature of the fluid. The increase in thermal performance (see Figs. 6.6 and 6.7) is substantially higher than the hydraulic performance (i.e. mass flow rate) of the tapered SAH device with rectangular cross-sectional shape inlet. The decrease in the mass flow rate limits the wide acceptability of the device for the high flow applications such as solar space heating, solar air dryer, and many others. To overcome this disadvantage the tapered SAH is integrated with bell-mouth shape inlet in order to enhance the mass flow rate by reducing the entry hydraulic losses (discussed later).

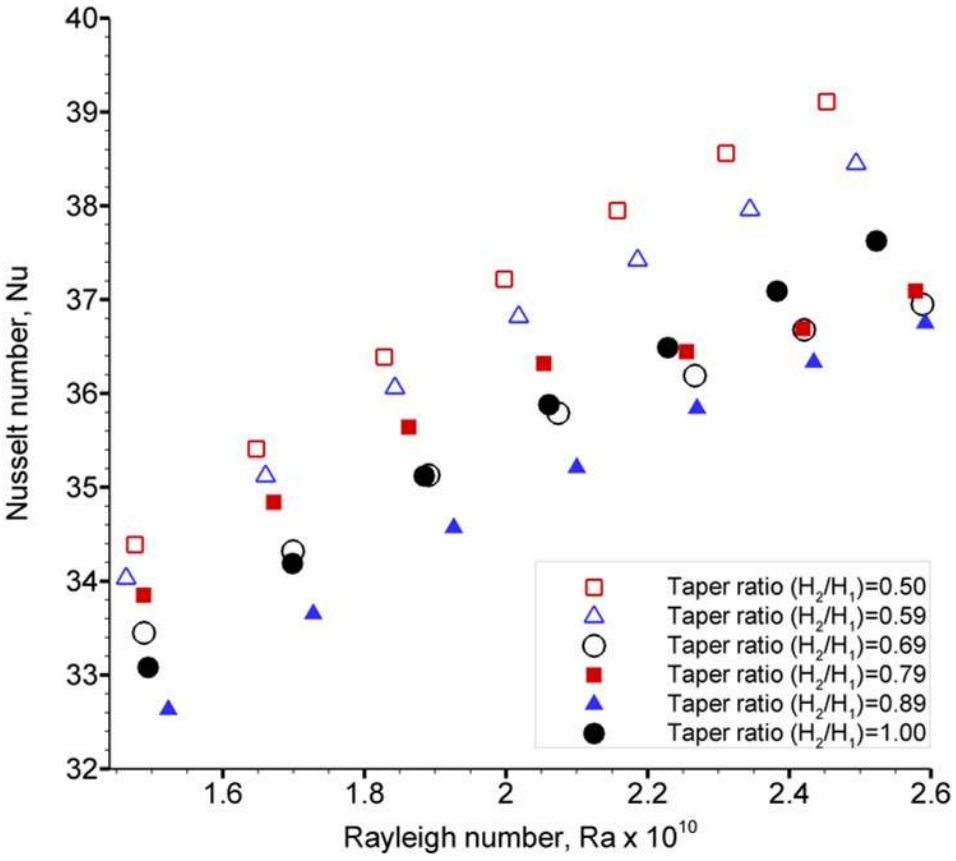

Figure 6.7: Variation of Nusselt number, Nu with Rayleigh number, Ra for tapered flow passage natural convective SAH of rectangular cross-sectional shape inlet.

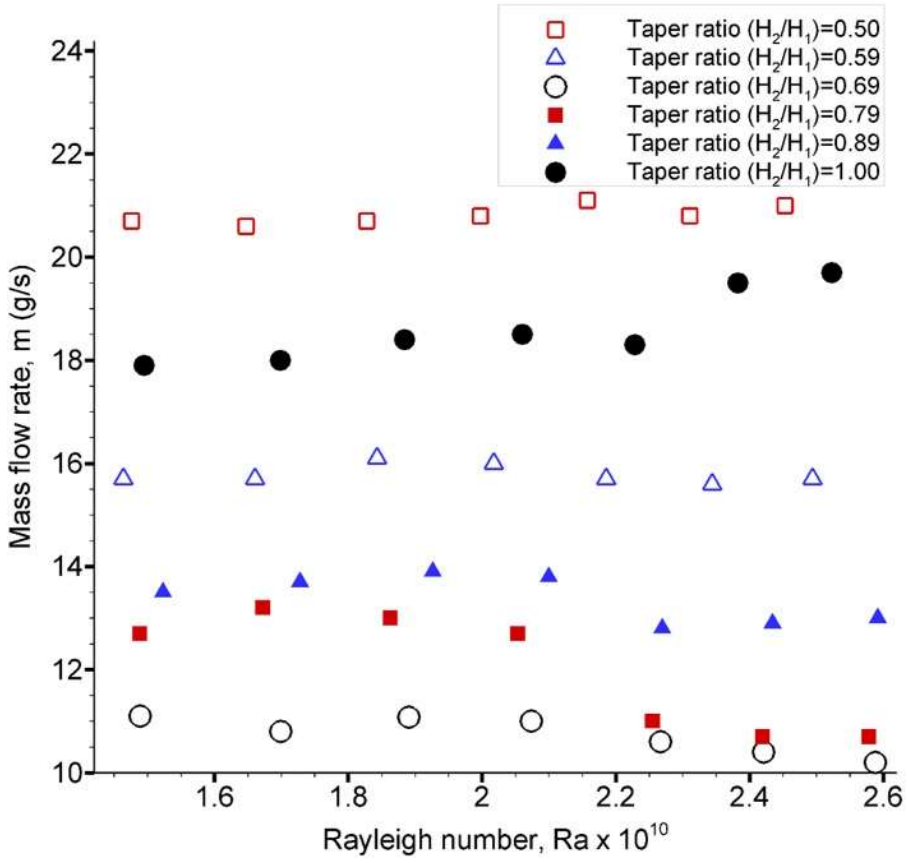

Figure 6.8: Variation of mass flow rate for tapered flow passage SAH with rectangular cross-sectional shape inlet for solar insolation range 500-1100 W/m^2.

Figure 6.9 shows thermal effectiveness variation with Rayleigh numbers of tapered flow passage natural convection SAH. The maximum average thermal effectiveness of taper ratio $H_2/H_1 = 0.69$ is about 70% higher than the conventional SAH design. In the case of tapered SAH, interaction of flow with the absorber plate of SAH is enhanced as the air flows through a gradually converging passage, and hence higher thermal effectiveness.

The pressure drop (ΔP) and Nusselt number per unit pressure drop NuP (i.e. Nu/ΔP) values for different SAH design configurations at q = 800 W/m^2 is shown in Table 6.3. The maximum percentage increase in ΔP for tapered SAH is 1.16%, which is insignificant in comparison to maximum percentage increase in thermal effectiveness. The corresponding increase in thermal effectiveness is about 70% for tapered SAH having taper ratio $H_2/H_1 = 0.69$ compared to conventional SAH design (see Fig. 6.9). The ratio NuP indicate the heat transfer capability of the flow from the hot absorber plate associated with hydraulic loss. The effect of higher NuP values can be observed in terms of higher outlet air temperature. The maximum percentage increase of about 6% in NuP was observed for tapered SAH having taper ratio $H_2/H_1 = 0.69$ (see Table 6.3) in comparison to conventional SAH design (see Table 6.3).

Table 6.3: (ΔP) and (NuP) values for tapered - natural convective SAH without bell-mouth at $q = 800$ W/m^2.

SAH ⇓	Prameter					
				(H_2/H_1)⇓		
Tapered	0.5	0.59	0.69	0.79	0.89	1
				(ΔP) in Pa⇓		
Tapered	29.64	28.88	27.63	28.1	28.04	29.3
				(NuP)⇓		
Tapered	1.25	1.27	1.28	1.28	1.25	1.21
				(ΔP) in Pa⇓		
Flat (conventional)				29.3		
				(NuP)⇓		
Flat (conventional)				1.21		

6.3.2 Hydraulic performance of tapered SAH with bell-mouth

In natural convection SAH, the buoyancy-driven flow arises due to density difference of the fluid. The inlet of a rectangular cross-sectional shape of conventional SAH reduces the flow velocity due to vortex formation [137]. Due to difference between the velocity near the heated plate and cold glass plate at the top, vortex form, which add to the system losses. The above reason put restrictions over the wider acceptability of naturally driven SAH device where high mass flow rate is the first priority. In this section, the hydraulic losses are minimized by introducing bell-mouth shape opening [109, 66, 137] at the inlet of the flow channel.

The different designs of bell-mouth have been simulated and optimized for the range of bell-mouth ratio $h/R = 0.1 - 0.6$ in the range of heat flux $500 - 1100$ W/m^2. Figure 6.10 shows the mass flow rate variation for various bell-mouth designs integrated at the inlet of conventional SAH. A significant increase of 25.1% in the mass flow rate is seen for the bell- mouth design having $h/R = 0.3$ and $R = 100\,mm$ (best bell-mouth design) compared to the conventional SAH design with rectangular cross-sectional inlet. In subsequent simulations, this best design of bell- mouth $h/R = 0.3$ and $R = 100\,mm$ was integrated with taper flow passage SAH to examine the thermo-hydraulic performance followed by comparison with the conventional SAH design.

Figure 6.11 demonstrates the variations of mass flow rate vs Rayleigh number for tapered SAH incorporated with bell-mouth shape opening at the inlet. Mass flow rate is considerably enhanced due to converging bell-mouth design [109, 66]. The maximum percentage increase of 313.4% in mass flow rate was observed for the tapered SAH having $H_2/H_1 = 0.89$ with bell-mouth shape $h/R = 0.3$ and $R = 100\,mm$, compared to conventional SAH design. From Fig. 6.12 it is observed that the mass flow rate enhanced considerably due to integration of bell-mouth shape. The increased mass flow rate is evaluated in terms of mass flow rate enhancement ratio, ($MER = \dot{m}_{tapered\,with\,BM}$ / $\dot{m}_{flat\,plate\,conventional}$). The increased MER values for tapered

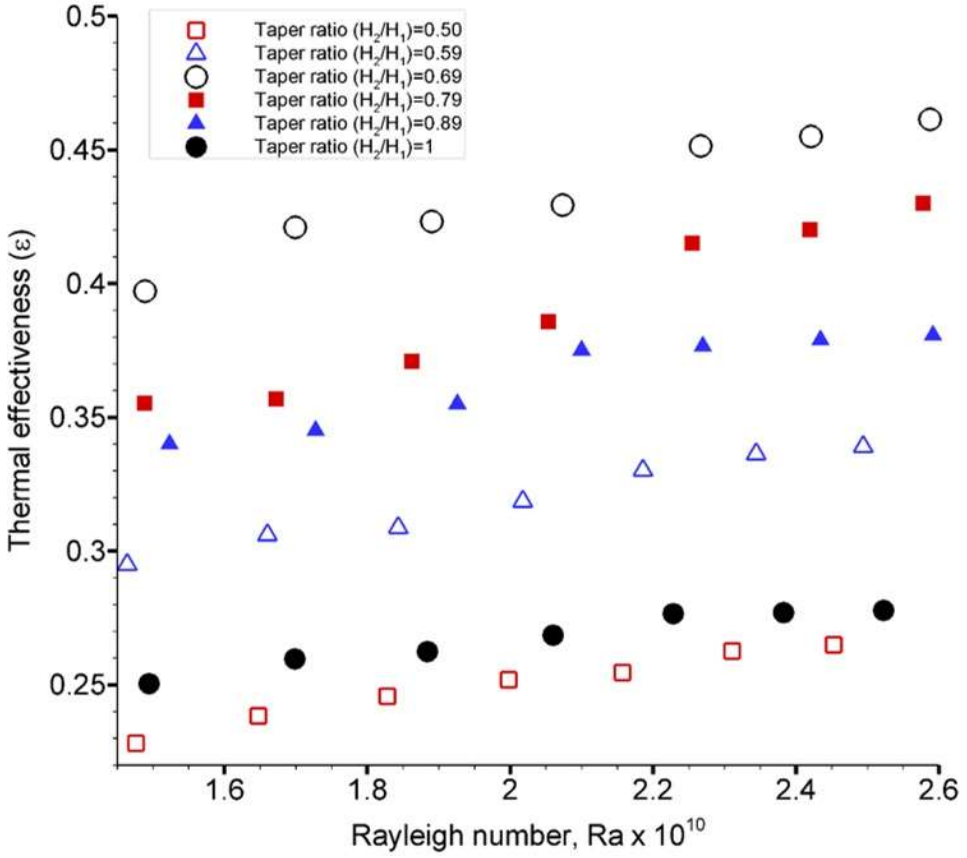

Figure 6.9: Variation of thermal effectiveness of flat tapered natural convection SAH vs. Rayleigh number for the range of $q = 500 - 1100$ W/m^2.

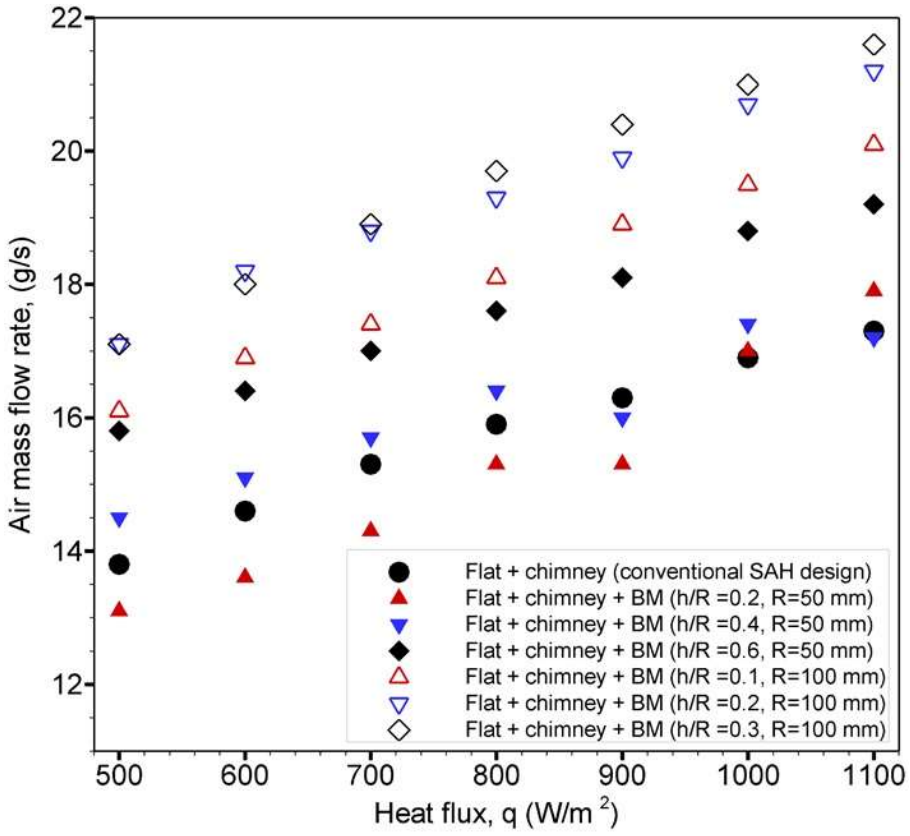

Figure 6.10: Mass flow rate variation for various bell-mouth shape inlet designs integrated with conventional SAH for the range of absorber heat flux $500 - 1100$ W/m^2.

SAH combined with bell-mouth design were found to be in the range of $2.5 - 4.2$. The maximum value of MER is associated with the tapered flow channel having taper ratio $H_2/H_1 = 0.89$ integrated with bell-mouth design with $h/R = 0.3$ and $R = 100\,mm$.

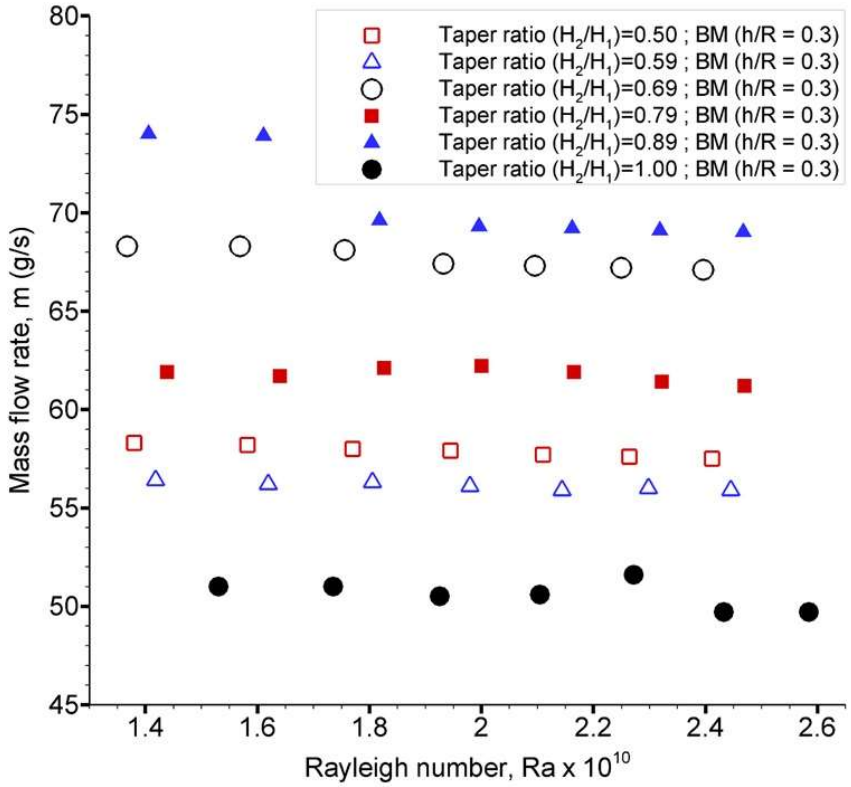

Figure 6.11: Mass flow rate variation with Rayleigh number for tapered SAH integrated with bell-mouth design inlet.

Figure 6.13 shows Nu variation with Ra of tapered SAH having bell-mouth inlet designs for the range of heat flux $500 - 1100$ W/m^2. Higher Nu values are seen for tapered natural convective SAH integrated with bell-mouth shape inlet than the conventional SAH. Higher Nu values signify increased flow velocity near the absorber plate. The increased flow velocity in the duct provides better interaction of cold fluid with the absorber plate and seen in terms of enhanced heat transfer rate.

Figure 6.14 shows velocity contours of (a) tapered SAH with bell-mouth integrated at the inlet and (b) conventional SAH with parallel flow passage, at q = 800 W/m^2. Air velocity gradually increases as the flow accelerates along the length of the flow channel. The reversed or separated flow was observed in case of conventional SAH design (refer Fig. 6.14(b)) which offers obstruction to the major portion of the upcoming flow in the SAH duct. The flow obstruction has been minimized by transforming parallel flow passage of conventional SAH into tapered flow passage and inlet integrated with bell-mouth shape opening. It has a substantial impact on the hydraulic performance. Combining bell-mouth opening at the inlet of tapered flow passage (refer Fig. 6.14(a)) increased the mass flow rate by about three times when compared to the conventional design (refer Fig. 6.14(b)). The flow is accelerated without undergoing separation at the entry of the flow passage due to bell shape opening at the SAH inlet of converging flow passage.

6.4 Correlations development

From the above results, it is clear that the thermal characteristics is a strong function of Ra and tapper ratios for natural convection SAH configurations. An independent correlation has been developed for the Nu variation with the influencing parameters i.e. Rayleigh numbers and taper ratios and it has the following form:

$$Nu = F_1[(Racos\theta), \frac{H_2}{H_1}] \tag{6.11}$$

The functional form of F_1 to be determined. To develop the relation of Nu with Ra, the logarithmic plot of

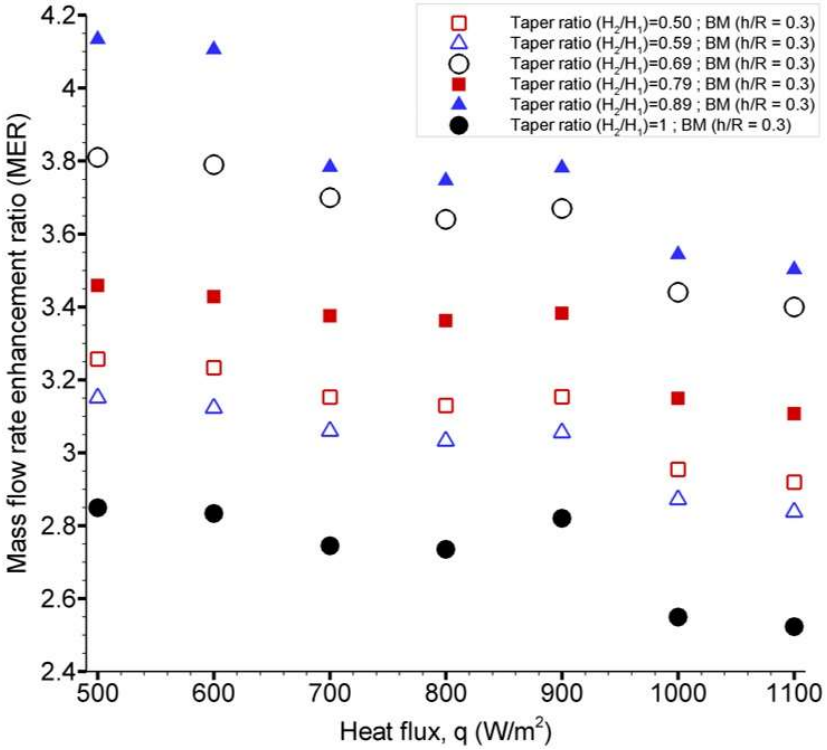

Figure 6.12: Variation of mass enhancement ratio (MER) of tapered SAH with bell-mouth shape inlet compared to the rectangular cross-sectional inlet of conventional SAH for the heat flux range $500 - 1100$ W/m^2.

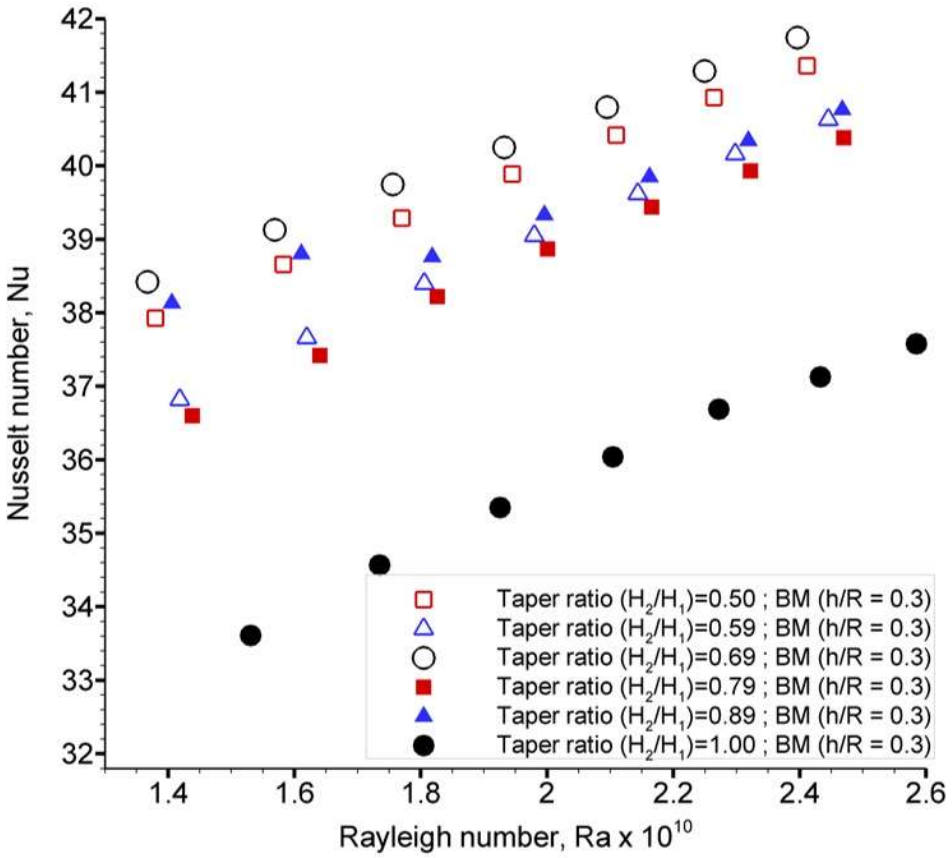

Figure 6.13: Plot of Nu vs. Ra variation for tapered SAH having bell-mouth design integrated at the inlet for the range of heat flux 500-1100 W/m^2.

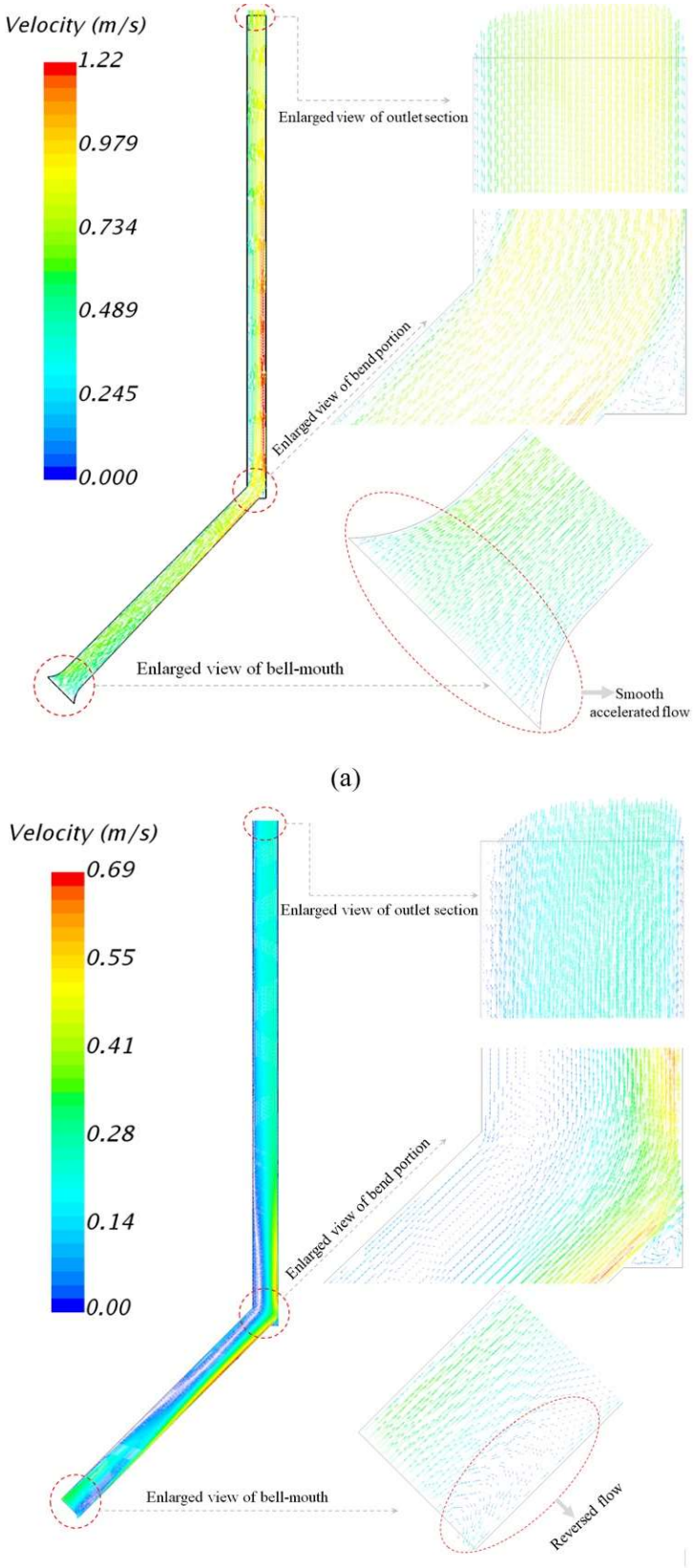

Figure 6.14: Velocity contour plot at heat flux 800 W/m^2: (a) tapered SAH (taper ratio = 0.69) integrated with bell-mouth ($h/R = 0.3$); (b) conventional SAH (parallel flow passage).

ln(Nu) vs. ln(Ra cosϑ) were obtained for Ra values for the range of q = 500–1100 W/m^2 as presented in Fig. 6.15. A linear connection between ln(Nu) vs. ln(Ra cosϑ) was obtained using the data points. We get,

$$ln(Nu) = ln(A_o) + a\, ln(Ra\, cos\theta) \tag{6.12}$$

The constant 'a' represent the exponent. Above linear equation has been determined from the data points of tapered SAH natural convection SAH using R-square method and presented in Fig. 6.15. We get,

$$ln(Nu) = A_1 + 0.2021\, ln(Ra\, cos\theta) \tag{6.13}$$

In above equation, A_1 denotes antilog of term A_o

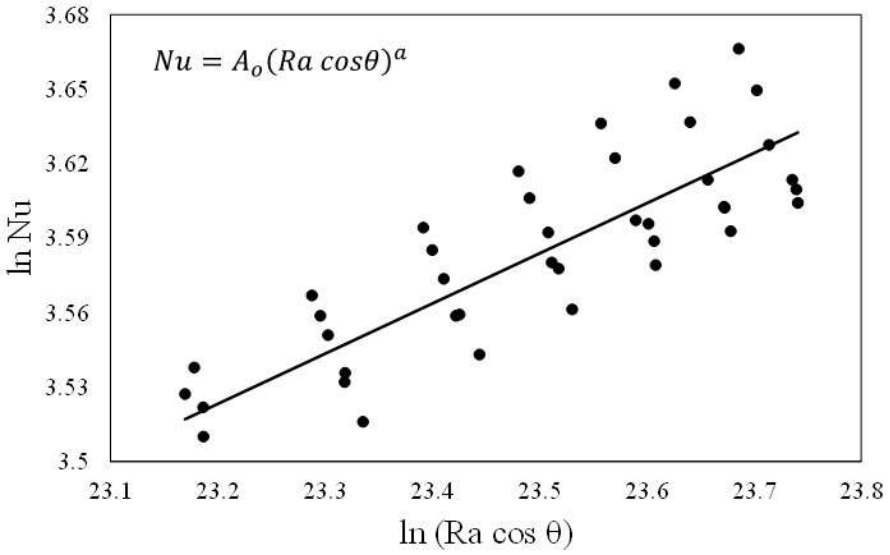

Figure 6.15: ln(Nu) vs. ln(Ra cosϑ) of tapered natural convection solar air heater.

Take antilog of Eq. 6.13, the equation is rewritten as,

$$Nu = A_o(Ra\, cos\theta)^a \tag{6.14}$$

where a = 0.2021
$A_o$is a function of Raleigh number (Ra cosϑ).

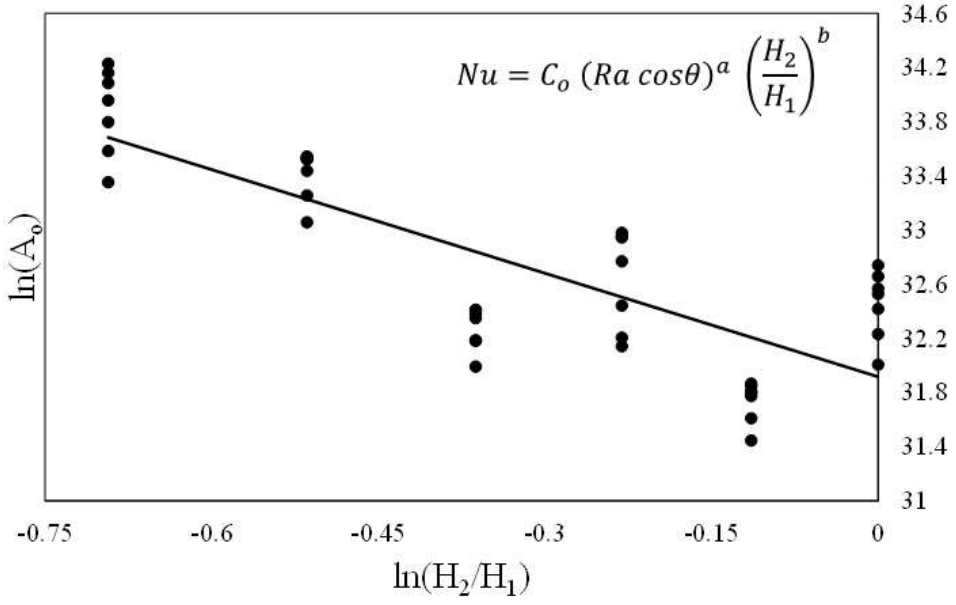

Figure 6.16: Plot of $ln(A_o)$ vs.$ln(H_2/H_1)$ of tapered natural convection SAH.

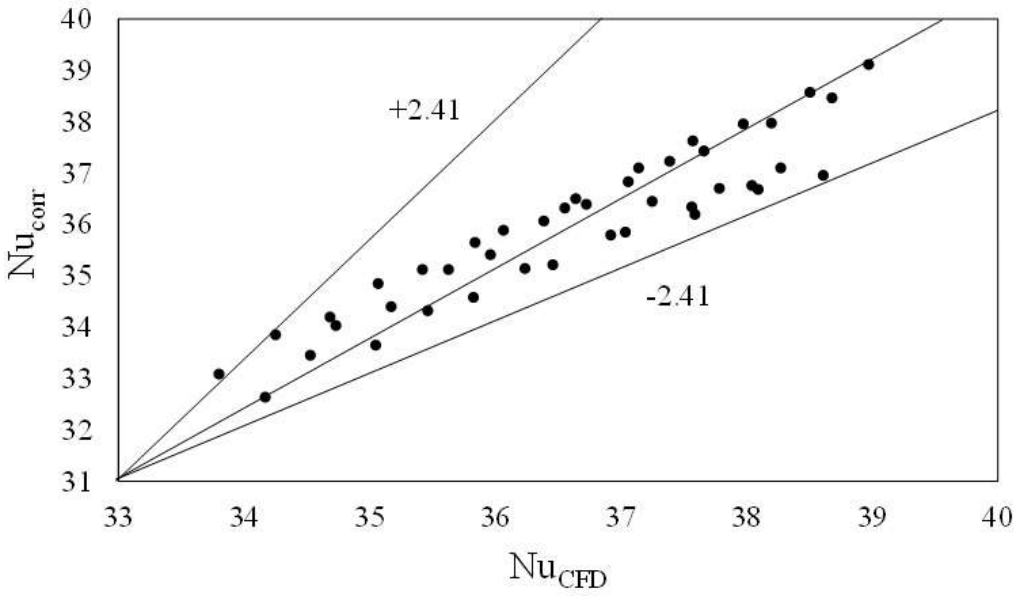

Figure 6.17: Variation of Nusselt number obtained by correlation (Nu_{corr}) and simulation (Nu_{CFD}) of tapered natural convection SAH.

To obtain relation among $ln(A_o)$ and $ln\left(\frac{H_2}{H_1}\right)$using all relevant data points, the variation is shown in Fig. 6.16 and the equation in the form:

$$A_o = B_o \left(\frac{H_2}{H_1}\right)^b \tag{6.15}$$

where coefficient $B_o = \frac{Nu}{(Ra\,cos\theta)^a (H_2/H_1)^b}$

The final correlation of Nusselt number variation has the following form:

$$Nu = C_o (Ra\,cos\theta)^a \left(\frac{H_2}{H_1}\right)^b \tag{6.16}$$

where $C_o = 0.3115$, $H_2/H_1 = taperratio$, $b = -0.061$, $and\, a = 0.2021$

Figure 6.17 shows the error associated with the developed correlation and the data obtained from the numerical model for tapered flow passage natural convection SAH. The maximum and minimum percentage error is in the range ± 2.41%.

6.5 Conclusion

Enhancing the thermo-hydraulic performance of a naturally driven solar air heater is a big challenge as both thermal and hydraulic performances comes at the expense of each other. Lower mass flow rates limit the device usage in the applications where high mass flow rate and medium temperature range are the major priority such as building heating, crop drying etc. In the present study new designs of tapered SAH and the effect of integrating bell-mouth shape at the inlet in augmentation of thermal and hydraulic characteristics were discussed in detail. Following key findings are drawn from the study:

1. Redesigning the conventional flat parallel flow channel design of SAH into tapered designs has a significant impact on enhancing the thermal performance of the device. Tapering resulted in better interaction of cold fluid with the thermal boundary layer near the absorber plate.

2. Tapered flow passage slightly hinders the upcoming heated fluid due to boundary layer interaction, and hence lowers the mass flow rate. The decrease in mass flow rate was compensated and further increased by incorporating the bell-mouth opening at the SAH inlet section.

3. Tapered flow passage increases the thermal effectiveness of the device by about 70% and enhances Nu per unit pressure drop i.e. NuP by about 6% compared to conventional SAH design.

4. The maximum increase of about 313% in mass flow rate was achieved by the integration of bell-mouth opening in tapered SAH having $t_c = 100\,mm$ for the design parameters $H_2/H_1 = 0.89$ and $h/R = 0.3$.

5. An individual relationship of Nusselt number as a function of Rayleigh number and taper ratio was obtained and it has the form $Nu = C_o\,(Ra\,cos\theta)^a \left(\frac{H_2}{H_1}\right)^b$, where a and b are constants. The obtained correlation was in good following with the numerical data with an average percentage deviance of 2.41%.

The present study was carried out with a hope of developing new ideas to design an efficient naturally driven solar air heater to increase the device acceptability in the areas where high mass flow rate of air at moderate temperature would be the desired characteristics of the SAH devices.